Computer Modeling in Engineering & Sciences CMES, vol.123, no.3, pp.1247-1266, 2020

Numerical Study on the Gas Leakage and Dispersion at the Street Intersection of a Building Group

Weitao Zhang[1, 2], Mengqi Liu[3], Kaiyi Wang[4], Fan Zhang[2] and Lei Hou[1, *]

Abstract: Accidents involving natural gas leakage and dispersion pose a significant threat to human life and property. This threat is especially relevant at the street intersection at which dense buildings, heavy traffic flow, and complex underground pipe networks meet. Scholars have conducted numerous studies on gas leakage and dispersion, but investigations of natural gas leakage and dispersion at the street intersection of a building group are not in-depth. In this paper, we presented a three-dimensional (3D) physical model based on the Computational Fluid Dynamic (CFD) methodology to study the natural gas leakage and dispersion at the street intersection of a building group. We validated the CFD methodology applied in the research based on the data from the field tests and wind tunnel experiments. Then, we simulated and analyzed the pressure, wind, and concentration of natural gas dispersion at the street intersection. The simulation results showed that vortex regions, low-pressure zones, and a building group effect could cause a build-up of natural gas concentration under perpendicular wind direction conditions. In addition, the area of hazardous region tended to increase first and then drop with the dispersion height. In the case of this study, the maximum area of hazardous region is 200 m^2 located in the height of 55 m, which is the middle plane in the computational domain. The results in the paper can provide scientific references for the safe operation and emergency-management decisions of municipal gas.

Keywords: Natural gas, computational fluid dynamic, building group, street intersection, leakage and dispersion, numerical simulation, concentration field.

1 Introduction

As a form of clean and friendly energy, natural gas has received increasing attention and has been used widely in recent years [Li, Cheng and Gu (2019); Lu, Ma and Azimi (2020); Wang and Lin (2017); NIGC (2019)]. Accidents involving gas leakage and dispersion, however, can pose a severe threat to human life and property [Li, Wang, Stevan et al. (2019); Han and Weng (2011)]. Data from China gas

[1] National Engineering Laboratory for Pipeline Safety, Beijing Key Laboratory of Urban Oil and Gas Distribution Technology, China University of Petroleum, Beijing, 102249, China.

[2] CangHaiBang Business Unit, Supply Chain Business Group, Sinochem Energy High-Tech Co., Ltd., Beijing, 100094, China.

[3] Sinopec Economics & Development Research Institute, Beijing, 100029, China.

[4] College of Arts and Science, Boston University, Boston, MA 02215, USA.

[*] Corresponding Author: Lei Hou. Email: houleicup@126.com.

Received: 30 November 2019; Accepted: 11 February 2020.

(http://www.chinagas.org.cn) showed that 373 accidents of gas leakage and explosion occurred in the first half-year of 2019 in China, causing 30 deaths and 301 injuries. According to the 10th report of the European Gas Pipeline Incident Data Group (EGIG), the highest fatality and injury rate involves those people who were directly involved in causing the accidents. Street intersections at which dense buildings, traffic flow and complex underground pipe networks meet are common in cities. The gas leakage and dispersion that occurs at these intersections can easily escalate into catastrophic events and result in significant loss of life and property. For example, the "11·22" Sinopec Donghuang oil pipeline explosion accident, caused by oil vapor dispersion following an underground oil transportation pipeline leak at a street intersection, killed 62 people, injured 136 people, and cost an economic loss of 75.72 million yuan. Thus, it is necessary to conduct a further study on natural gas leakage and dispersion for the safety of people's life and property.

To data, numerous laboratory experiments [Bonnaud, Cluzel, Corcoles et al. (2011); Mao, Wang, Zhou et al. (2019)] and field measurements [Okamoto and Gomi (2011); Foissac, Benoit, Blanchetiere et al. (2014)] have been carried out to reveal the characteristics of gas dispersion after leakage from pipelines. Many previous studies have focused primarily on gas dispersion after leakage from the buried pipes, which have provided the appropriate methodology for risk and consequence assessment [Houssin-Agbomson, Blanchetière, McCollum et al. (2018)]. Laboratory experiments and field tests, however, can only obtain data from a limited number of measurement points from specific scenarios, which do not adequately describe gas leakage and dispersion under different conditions. Recently, with improvements in computational capacities, numerical simulation has emerged as an alternative. These improvements allow for simulation over real geometry, including terrain with obstructions, transitions, varying boundary, and atmospheric conditions, which have made up for experimental deficiencies.

In terms of calculation models, correlations considering the length of the pipeline have been developed, which can be applied to determine the amount of gas leakage from aboveground or underground pipelines [Ebrahimi-Moghadam, Farzaneh-Gord, Arabkoohsar et al. (2018); Ebrahimi-Moghadam, Farzaneh-Gord and Deymi-Dashtebayaz (2016)], the three-dimensional (3D) model was proved to be superior to the two-dimensional (2D) model simulation of natural gas dispersion [Deng, Hou, Fang et al. (2017)]. In addition, essential factors, such as terrain, buildings, atmosphere, and the turbulence model, have been evaluated and analyzed based on the computational fluid dynamic (CFD) methodology [Liu, Liu, Lu et al. (2016); Liu, Huang, Li et al. (2018); Guo, Zhao, Wang et al. (2019); Lateb, Masson, Stathopoulos et al. (2013)]. For a comprehensive summary of the realistic accident scenario, CFD numerical techniques were used to study the consequences of the East Harlem gas explosion in Manhattan. The gas dispersion, blast wave, and flame propagation process were simulated and analyzed, and the simulation results achieved better agreement with the actual destruction in the real accident [Wang, Shi, He et al. (2019)].

Although many scholars have conducted numerous studies on gas leakage and dispersion, most of the numerical models are based on assumptions and simplified conditions, and some studies still have limitations [Ahmed, Bengherbia, Zhvansky et al. (2016)] and generally are not applicable to the geometry in real scenarios. Investigations of natural

gas leakage and dispersion on the nearly real scale are not comprehensive and systematic, especially at the street intersections of building groups.

In this research, we developed a 3D numerical model to simulate the natural gas dispersion after leakage at the street intersection of a building group based on CFD methodology. We validated the CFD methodology based on the data from previous field tests and wind tunnel experiments, which conducted by scholars on the wind field surrounding the Texas Tech University (TTU) building and the concentration field in the street canyon, respectively. Then, we simulated the pressure, wind, and concentration of natural gas dispersion at the street intersection of a building group. This gas leakage accident occurred in 2015 at Feiyun Jiang Intersection of Qianjiang Road, Hangzhou, China. We conducted an in-depth analysis of the influence of pressure and wind on concentration distribution and identified the hazardous region caused by gas dispersion. The simulation results provided scientific references for the safe operation of a response and for emergency-management decisions pertaining to a municipal gas accident.

2 Methodology

Influenced by buildings and other obstacles, the wind field in low-rise space has a turbulent flow. The mass, momentum, and energy are transferred by mixing when gas is dispersed after leakage in a building group environment. The concentrations vary with time and space. Governing equations used to predict the gas leakage and dispersion, including mass, momentum, energy, and species transport equation, can be coupled with the turbulence model.

2.1 Governing equations

The fundamental governing equations can be expressed in the following differential forms:

Continuity equation:

$$\frac{\partial \rho}{\partial t}+\frac{\partial}{\partial x_i}\left(\rho u_i\right)=0 \tag{1}$$

where ρ is the density of fluid, kg·m^{-3}; and u_i represents the mean velocity components in the x_i directions, m·s^{-1}.

Momentum equation:

$$\frac{\partial}{\partial t}\left(\rho u_i\right)+\frac{\partial}{\partial x_j}\left(\rho u_i u_j\right)=-\frac{\partial p}{\partial x_i}+\frac{\partial \tau_{ij}}{\partial x_j}+\rho g_i \tag{2}$$

where g_i is the gravitational acceleration in x_i directions, m·s^{-2}; and p and τ_{ij} represent the mean pressure and viscosity strain tensor of the fluid, respectively, Pa.

Energy equation:

$$\frac{\partial}{\partial t}\left(\rho E\right)+\frac{\partial}{\partial x_i}\left[u_i\left(\rho E+p\right)\right]=\frac{\partial}{\partial x_i}\left[k_{eff}\frac{\partial T}{\partial x_i}-\sum_{j'}h_{j'}J_{j'i}+\left(\tau_{ij}\right)_{eff}u_j\right] \tag{3}$$

where E is the total specific energy, $E = e + \frac{1}{2}u^2$; e is the specific energy, J·kg^{-1}; k_{eff} is the effective thermal conductivity, W·m^{-1}K^{-1}; and $h_{j'}$ is the enthalpy of species j', J·kg^{-1}.

Species transport equation:

When simulating the gas dispersion in the atmosphere, the species transport equation is selected and the term of the chemical reaction is neglected, as follows:

$$\frac{\partial}{\partial t}\left(\rho Y_{j'}\right) + \frac{\partial}{\partial x_i}\left(\rho u_i Y_{j'}\right) = \frac{\partial J_{j'i}}{\partial x_i} \tag{4}$$

where $Y_{j'}$ is the mass fraction of species j', %; and $J_{j'i}$ is the diffusion flux of species j' in x_i directions, kg·m^{-2}·s^{-1}. In the turbulent flow, $J_{j'i} = -(\rho \mathrm{D}_{j',m} + \frac{\mu}{\mathrm{Sc}_t})\frac{\partial}{\partial x_i}\left(Y_{j'}\right) - D_{T,j'}\frac{1}{T}\frac{\partial \mathrm{T}}{\partial x_i}$, where $\mathrm{D}_{j',m}$ is mass diffusion coefficient of species j'; $D_{T,j'}$ is thermal diffusion coefficient of species j'; μ is the turbulent viscosity; and Sc_t is the turbulent Schmidt number, the default value of Sc_t is 0.7.

Turbulence model:

Compared with the other turbulence models, the Realizable *k-ε* model can provide an accurate prediction about the flow surrounding a plane and jets and also has shown an improvement in computational convergence. The numerical simulation found that the Realizable *k-ε* model has better accuracy than the Standard *k-ε* model in its ability to calculate concentration distribution, and it is more consistent with the experimental results in the prediction of concentration fluctuations [Tauseef, Rashtchian and Abbasi (2011)]. Therefore, we applied the Realizable *k-ε* model to simulate the gas dispersion after leakage, *k* and *ε* equations in the Realizable *k-ε* model are shown as follows:

$$\frac{\partial}{\partial t}\left(\rho k\right) + \frac{\partial}{\partial x_j}\left(\rho k u_j\right) = \frac{\partial}{\partial x_j}\left[\left(\mu + \frac{\mu_t}{\sigma_k}\right)\frac{\partial k}{\partial x_j}\right] + G_k + G_b - \rho\varepsilon - Y_M + S_k \tag{5}$$

$$\frac{\partial}{\partial t}\left(\rho \varepsilon\right) + \frac{\partial}{\partial x_j}\left(\rho \varepsilon u_j\right) = \frac{\partial}{\partial x_j}\left[\left(\mu + \frac{\mu_t}{\sigma_\varepsilon}\right)\frac{\partial \varepsilon}{\partial x_j}\right] + \rho C_1 S\varepsilon - \rho C_2 \frac{\varepsilon^2}{k + \sqrt{v\varepsilon}} + C_{1\varepsilon}\frac{\varepsilon}{k}C_{3\varepsilon}G_b + S_\varepsilon \tag{6}$$

where $Y_{j'}$ is the mass fraction of species j', %; $J_{j'i}$ is the diffusion flux of species j' in x_i directions, kg·m^{-2}·s^{-1}; σ_k and σ_ε are the corresponding Prandtl Numbers of *k* and *ε*; C_2, $C_{1\varepsilon}$, and $C_{3\varepsilon}$ are the default empirical constants. These parameters are always obtained by the fitting results of typical flow experimental and some calculations. The recommended model value of σ_k, σ_ε, C_2, $C_{1\varepsilon}$, and $C_{3\varepsilon}$ are 1.0, 1.2, 1.9, 1.44, and 1.3, respectively.

2.2 Numerical methods

For a 3D numerical model, if the size of the grid reduces by half, the quantity will

increase eight times that of the original. This increase will lead to the calculation of time-consuming work. It also causes the calculation of some optional parameters that are unimportant in the study. Thus, the total number of the grid should be controlled and the calculation speed and accuracy also should be ensured at the same time. Although part of the computational grids should be reduced, the number of the grid in the critical area also should be refined. We optimized the grids using multiblock patched grid technology and the self-adaption grid method, which enabled us to transfer information between two adjacent interfaces and reduce the grid quantity, respectively.

We used a pressure-based solver to solve the gas dispersion. A second-order upwind scheme, central difference scheme, and implicit scheme were specified for the convection term, diffusion term, and time term, respectively. We used the inviscid air fluid to first initialize the computational domain. Meanwhile, the governing equations were discretized by the first-order upwind scheme during the calculation process until convergence. Then, we applied a second-order upwind scheme and used relaxation factors to solve the pressure, velocity, turbulent kinetic energy, and turbulent dissipation rate for each time step. Last, the convergence depended on whether the residual curve was constant and the mass was conserved at the inlet and outlet boundary. We set the residual in two of the iterations of the continuity equation to be 10^{-5}, and the relative error of the mass at the inlet and outlet boundary must be less than 5%. If all of these conditions remained constant, we regarded the calculation as a convergence.

3 Validation

Many key factors affect gas dispersion after leakage in the ambient air [Zhu, Mao, Wang et al. (2013)]. Wind is one of the most important factors that affects natural gas dispersion [Deng, Hu, Yu et al. (2018)]. For practical purpose, we simulated the wind field surrounding the TTU building and the gas dispersion in the urban street canyon against measured data.

3.1 Validation of wind field simulation

An earlier TTU building field test was conducted at Texas Tech University to study the effects of wind on low buildings [Levitan and Mehta (1992)]. This field test has become an international standard model for evaluating wind-tunnel experiments. The building dimensions were 13.7 m × 9.1 m × 4.1 m, and it was anchored to a rigid frame undercarriage. This research used hydraulic jacks and a pair of electric motors to raise and rotate the building. The researchers considered the wind direction to be 0° when the flow was along the centerline toward the front of the building. The wind direction increased in a clock-wise direction. These tests acquired data from 11 pressure measurement taps, which were installed on the roof and two walls of the building. The number of tap locations were 42204, 42206, 42212, 50123, 50823, 51423, 52323, 52923, 22312, 22306, and 22304, for the wind direction ranging from 270° to 90° (see Fig. 1).

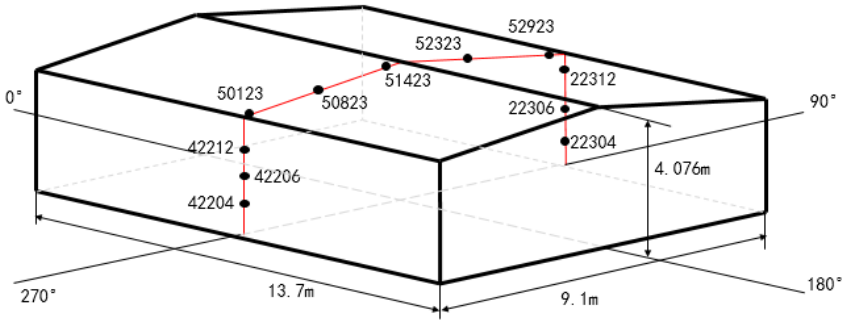

Figure 1: The TTU building model and pressure tap locations

We simulated the wind field surrounding the TTU building using the Realizable k-ε model. We calculated the mean pressure coefficients, which were used to evaluate the simulated results, as $C_p = 2(p - p_0)/\rho u_0^2$, where p is the mean pressure of taps; p_0 is reference pressure at free flow and considered to be the pressure at the approach flow along the centerline; u_0 is the approach wind velocity at the building height; and ρ is the density. For the wind direction of 270°, we validated the simulated results based on the data from the field tests at the TTU building [Selvam (1997)] and the wind-tunnel experiments at the University of Western Ontario [Endo, Bienkiewicz and Ham (2006)] (see Fig. 2).

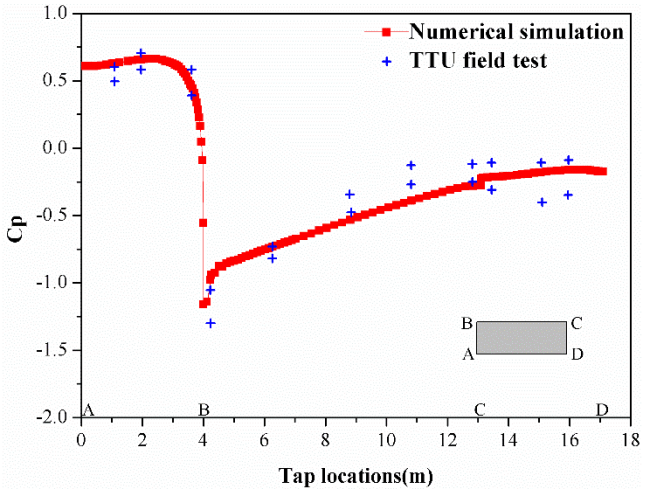

(a) Comparison with field tests

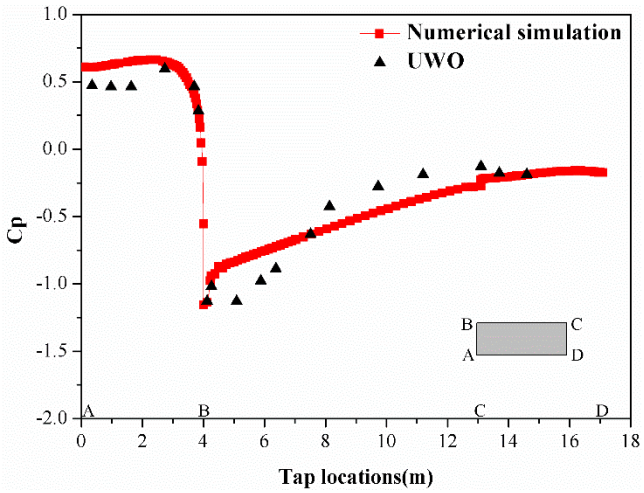

(b) Comparison with wind-tunnel experiments

Figure 2: Mean pressure coefficients at midplane locations, for a wind direction of 270°

The calculations of the mean pressure coefficient agreed well with field tests and wind tunnel experiments at taps 42204, 42206, and 42212. Because of the wind flow separation, attachment, rotating vortex, and other complex flow patterns on the roof surface and leeward side of the building (see Fig. 3), we found a slight discrepancy at taps 50123, 50823, 51423, 52323, 52923, 22312, 22306, and 22304. The mean relative error was 25.8% and 28.0% compared with field tests and wind tunnel experiments, respectively. The mean pressure coefficients were positive on the windward side of the building, as a result of a flow separation, and were negative on the top surface and leeward side of the building. The results confirmed the Realizable k-ε model was able to simulate the turbulent flow around the buildings.

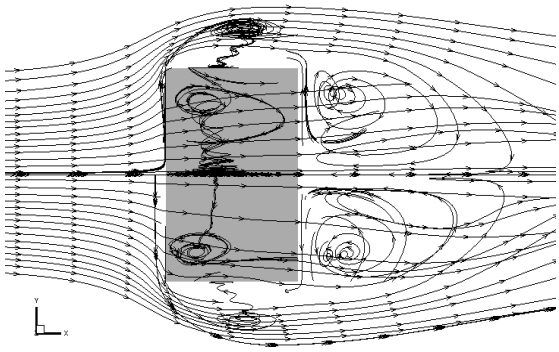

(a) Top view

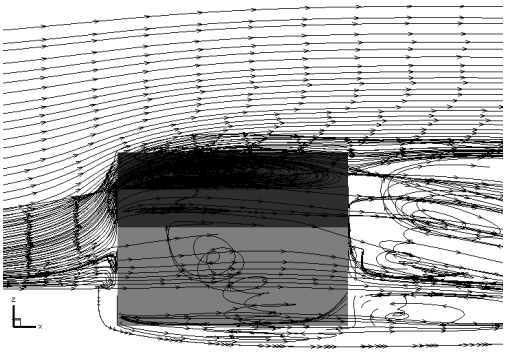

(b) Side view

Figure 3: Streamlines of flow field surrounding the building

3.2 Validation of gas dispersion simulation

An earlier pollutant dispersion experiment was conducted in the street canyon in the wind tunnel of the Institute of Hydrology and Water Resources, University of Karlsruhe, Germany [Kastner-Klein and Plate (1999)]. The investigated street canyon configuration is schematized in Fig. 4. The ratio of the model building height and a typical average building height in urban areas was 1:150. The researchers used two rectangles to simulate the multistory flat-roofed buildings. The geometrical parameters of the buildings were as follows: H=12 cm, L=180 cm, B=12 cm, and W=12 cm. Lines A and B along the street-canyon represented pollutant sources. They measured concentrations on the leeward side of building I, the windward side of building II, and the roof surfaces. The sampling points were located at z/H=0.083~0.83, where z is the elevation from the ground.

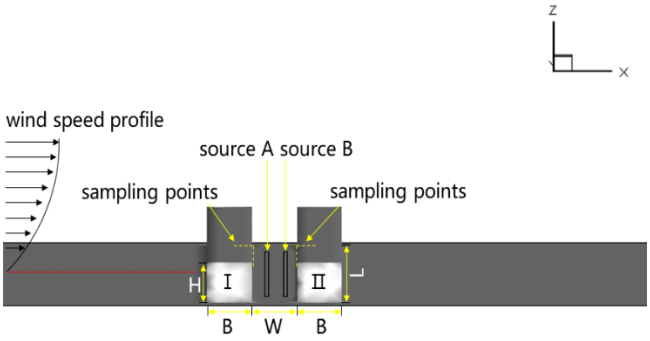

Figure 4: Schematic of experiment equipment for street-canyon study

The vertical velocity profile in the approach flow can be described by the power law: $u_z = u_{100}(z/100)^{0.23}$, where u_z is the velocity at the height of z; and u_{100} is the reference velocity at the height of 100 m (in the nature), u_{100}=7.7 m/s. We simulated the pollutant dispersion by methane (CH_4). We used the species transport model and controlled the boundary parameter variation by a user-defined function during the simulation.

The measured concentrations were normalized as follows: $K_c = \phi_i u_{100} HL/q$, where ϕ_i is the volume fraction of pollutant; H is the height of building; L is the length of line source; and q is the volume flow rate of source A or source B. If the conditions do not change, the calculated results of $u_{100}hl/q$ remains constant. The dimensionless concentration $Rc = \phi_i/\phi_{0.083}$ is regarded as the evaluation parameter, where $\phi_{0.083}$ is the volume fraction of pollutant on the windward side of building II, and the sampling point is located at z/H=0.083.

Fig. 5 shows the calculated results and the wind tunnel experimental data at 14 sampling points. We found that the calculated results agreed well with the experimental results on the windward side of building II. The calculated results had a slightly larger deviation with the experimental results on the leeward side of building I, which mainly came from the sampling points near the ground. Fig. 5(a) shows concentrations for wind direction 90° and source A. The maximum and the average relative error on the leeward side of building I were 21.12% and 12.15%, respectively, whereas the maximum and the average relative error on the windward side of building II were 5.74% and 3.49%, respectively. Fig. 5(b) shows the concentration values for wind direction 90° and source B. The maximum and the average relative error on the leeward side of building I were 16.72% and 10.81%, respectively, whereas the maximum and the average relative error on the windward side of building II were 5.77% and 3.72%, respectively.

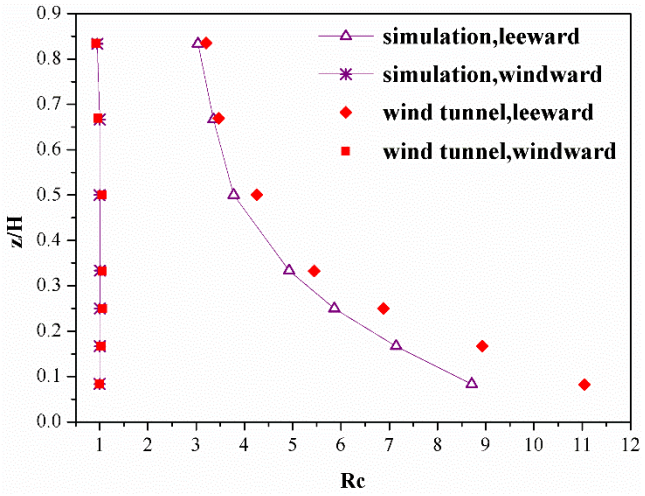

(a) Source A

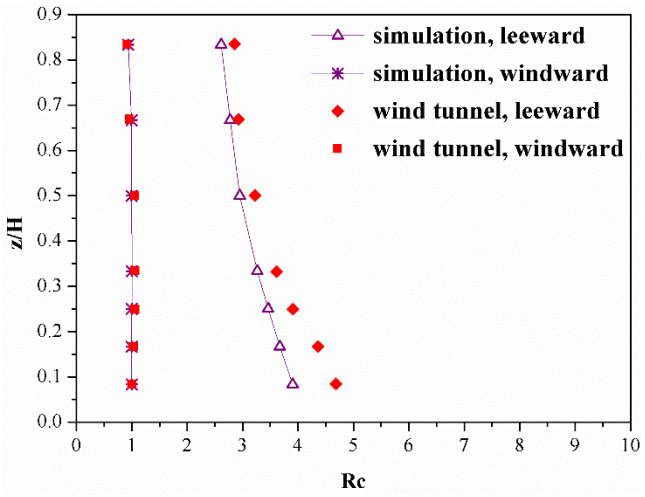

(b) Source B

Figure 5: Comparison of dimensionless concentrations *Rc* in the case of sources A and B

Overall, the numerical simulation results agreed well with the wind tunnel results. These reasonably good agreements demonstrated that the numerical simulation methods applied in this study performed well in the simulation of wind fields and concentration fields. Despite some simulation-measurement differences, the numerical approach was capable of a gas dispersion evaluation with sufficient accuracy.

4 Application

In August 2015, a natural gas leakage accident occurred at Feiyun Jiang Intersection of Qianjiang Road, Hangzhou, China. A large amount of grey and black gas released from the accident scene and the gas dispersion height was more than 20 stories high, as shown in Fig. 6. The accident caused the gas service to shut down and affected nearly 3000 gas-using residents. Because people were evacuated in time and traffic control enforced, no casualties were reported. Because this accident of gas leakage occurred at the street intersection, we conducted studies to investigate the gas leakage and dispersion at the street intersection of this building group. Sections 4.1, 4.2, and 4.3 provide a realistic example of the scene analysis.

(a) Top view (b) Side view

Figure 6: The gas release and dispersion scene at Feiyun Jiang Intersection, Hangzhou

4.1 Physical model

4.1.1 The computational domain

We created the physical model drawing on a 3D geometric model of Feiyun Jiang Intersection (see Fig. 7(a)). The model had approximately the same dimensions as the actual intersection without any scaling. Objects in the box and arc type were used to represent the different building items. The origin of the leak was located at the ground level, which was simplified to the surface source model with a diameter of 0.2 m. The relative positions and dimensions of the building are available online at http://hangzhou.map456.com. The computational domain was 311 m long, 286 m wide, and 111 m high, as presented in Fig. 7(b).

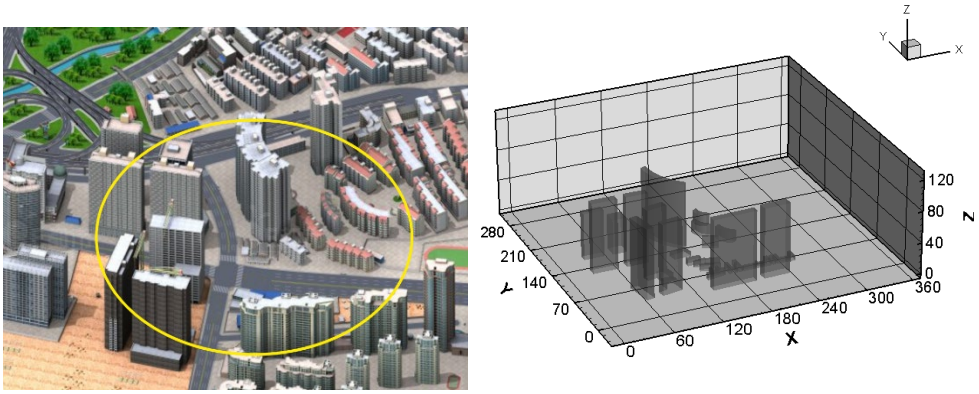

(a) The 3D geometric model (b) Simplified numerical model

Figure 7: The 3D numerical model for gas dispersion

4.1.2 Computational grid

Because of variations in the pressure gradient and the velocity gradient, we refined the grid near the origin of the leak, building walls, and ground surface to ensure the accuracy of our calculation. The more computational nodes included, however, the lower the computational speed was in the simulation. Thus, to reduce the total number of grids used in the 3D numerical model and to ensure calculation accuracy at the same time, we used the techniques of the multiblock patched grid and self-adaption grid method. We applied the expansion factors to control the grid interval variation in the X, Y, and Z directions. The grid arrangements of the computational domain are displayed in Figs. 8 and 9.

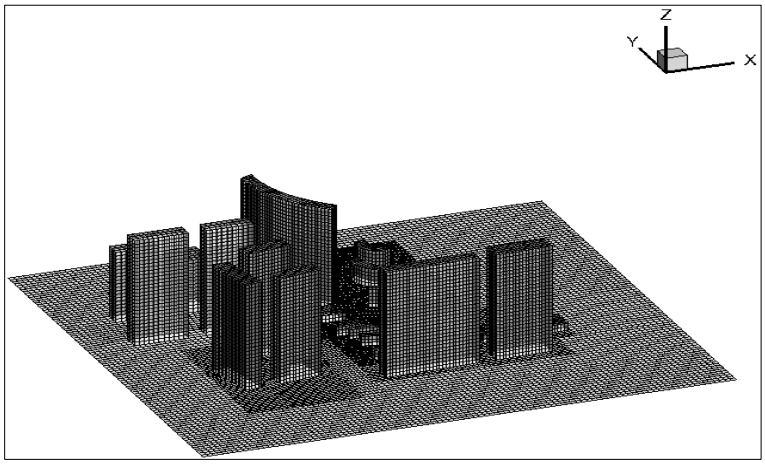

Figure 8: The 3D view mesh of Feiyun Jiang Intersection

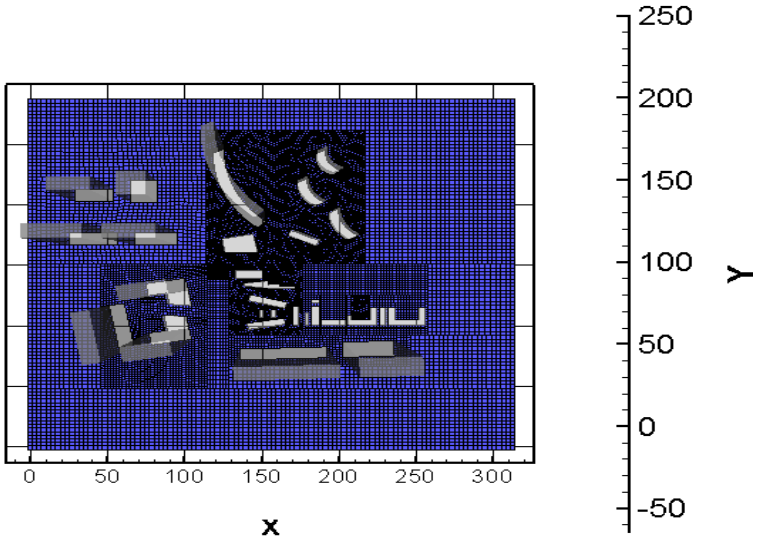

Figure 9: Grid at the height of 1.5 m from the ground

4.2 Boundary conditions

Boundary conditions are crucial for numerical simulation. According to the real situation of gas leakage and dispersion at Feiyun Jiang Intersection, the boundary conditions included the inlet, outlet, top, two-sides, the leak origin, the walls of buildings, and ground surface. We defined the inlet and outlet as the velocity inlet and outflow, respectively. The wind speed was set to 2.5 m/s, the wind direction was parallel to the X-direction, and the temperature was 20°C. The leak origin was also defined as velocity inlet, the natural gas leakage was considered to be a stable incompressible process with the velocity set to 300 m/s, the natural gas temperature was 25°C, and the methane mass fraction was 100% where the leak originated. The ground and building surfaces used no-slip boundary conditions. The top and two-sides of the computational domain were the symmetrical boundaries. We used similar convergence criterion, as mentioned in numerical methods, here.

4.3 Results and analysis

The field of pressure, wind, and concentration are analyzed at the height of 1.5 m from the ground, which is generally the height of human breathing. Analysis on this height can provide a valuable reference for people to evacuate in case of natural gas leakage and dispersion.

4.3.1 The pressure field and wind field at the street intersection

The results of pressure and wind field are shown in Figs. 10 and 11, respectively, at a height of 1.5 m from the ground. The blue and red colors represented maximum and minimum pressures, respectively (see Fig. 10). The negative pressure was distributed over large areas in the northeast of the computational domain, when the wind flow was perpendicular to the windward side of the building. The absolute value of the negative pressure in the northeast was higher than it was in other regions.

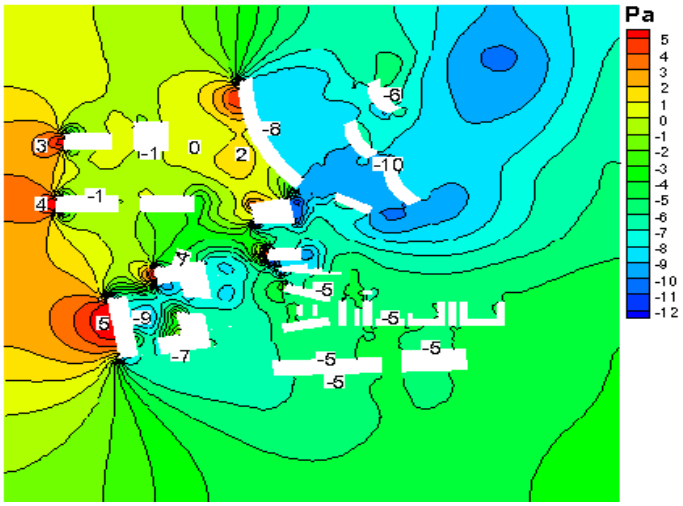

Figure 10: 2D cut plane of pressure field at the height of 1.5 m from the ground

The wind speed increased in the range from 2.5 m/s to 4 m/s, and even to 4.5 m/s, when the approaching flow passed between buildings on both sides of the road at the street intersection. The flow patterns were complicated (see Fig. 11). Influenced by the buildings in the northeast of the intersection, several large vortexes formed on the leeward side of the buildings. Some small vortexes also formed on the leeward side of buildings upwind of the leak's origin. The gas dispersion was trapped easily by these vortexes. Thus, if a natural gas leakage accident occurred, people around the scene should be evacuated rapidly from these regions in sufficient time.

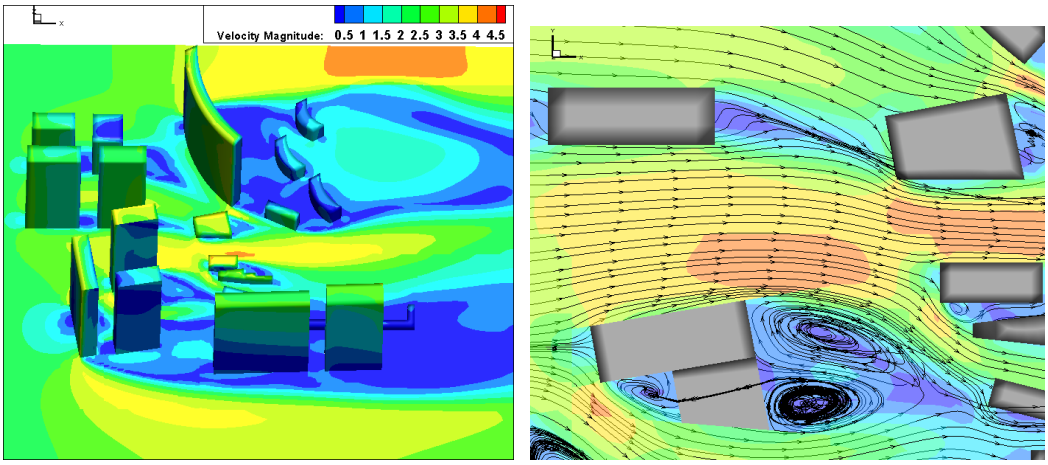

(a) Velocity contour (b) Velocity stream

Figure 11: Velocity field at the street intersection

4.3.2 Gas concentration distribution at the street intersection

The dispersion scenarios at the street intersection are shown in Fig. 12, at a height of 1.5 m from the ground. The initial stage was the dispersion period from 0 to 120 s. Because of wind pushing, the natural gas dispersion was mostly in front of the downwind direction. Because of the natural gas trapped by rotating vortexes in the southern part of the intersection, low concentrations began to appear in these regions. As the leakage time increased, the gas dispersion had a tendency to gather closer to the leak's origin, vortex regions, low-wind-speed regions downwind of the leak's origin, and negative pressure regions. Although natural gas began to build up in the upper right part of the leak's origin, it was quickly blown away by high-speed wind. Thus, the area and direction of gas dispersion could be anticipated according to the pressure field or the wind field in a building group environment.

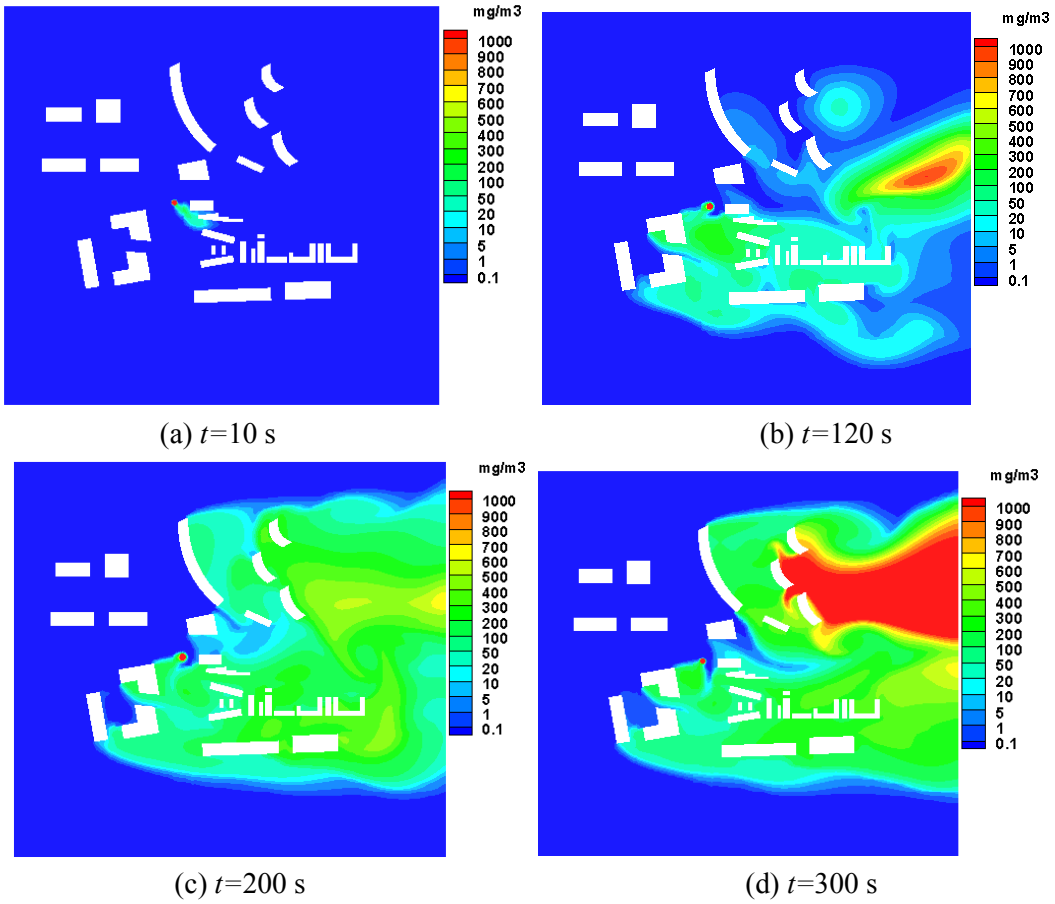

(a) t=10 s (b) t=120 s

(c) t=200 s (d) t=300 s

Figure 12: Natural gas dispersion concentration field at the leakage time

The concentration field of natural gas leakage and dispersion at t=300 s is shown in Fig. 13, at heights of 5 m, 20 m, 35 m, and 90 m from the ground. Influenced by the wind and buildings, the natural gas began to drift away and migrated to the downwind direction at a height of 30 m from the ground. At the leeward side of the downwind buildings where the leak originated, and near the domain's outlet regions, the concentration distribution and dispersion range tended to increase first and then drop with the dispersion height.

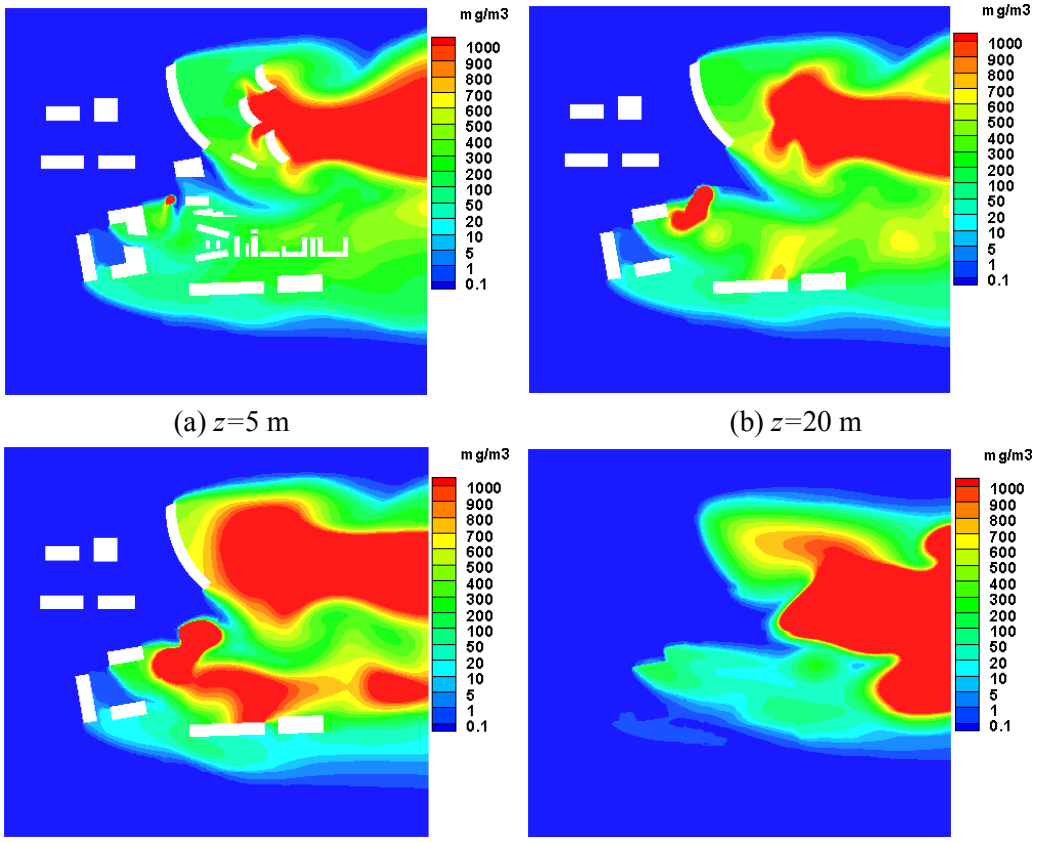

(a) z=5 m (b) z=20 m

(c) z=35 m (d) z=90 m

Figure 13: Natural gas concentration field after leakage 300 s

When the volume of methane in the air ranged from 5% to 15%, a fire or explosion accident would occur once it encountered an ignition source. Therefore, we considered the area where the methane concentration was above 5% to be hazardous. Fig. 14 shows the contour plot of the 5% methane iso-surface at the different heights. It is evident that the area of hazardous region tended to increase first and then drop with the dispersion height.

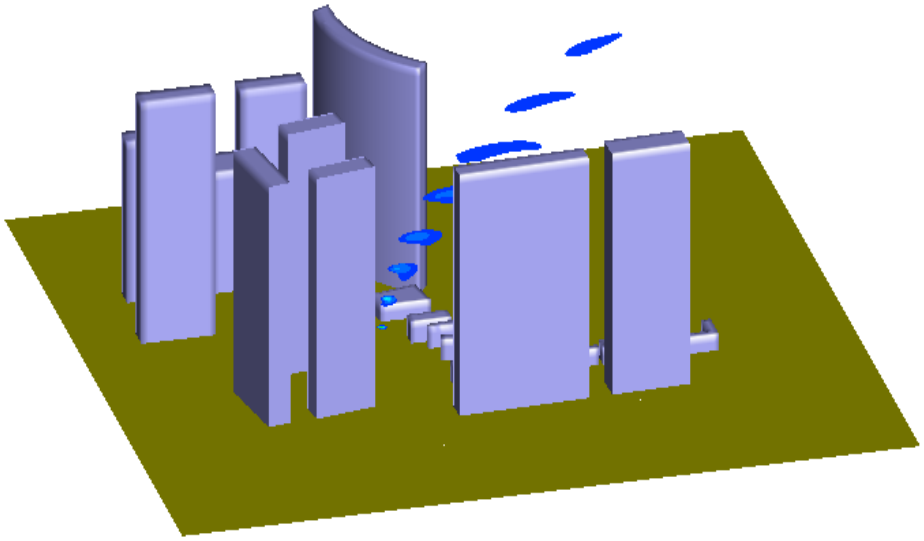

Figure 14: The contour of volume fraction at different heights

Tab. 1 shows the results variations in the area of hazardous region according to different heights. In this study, the area of the hazardous region above 100 m^2 was distributed mainly between the heights of 30 m and 70 m. The maximum area of the hazardous region was 200 m^2 and was distributed at a height of 55 m, which was in the middle of the computational domain.

Table 1: Variations in the area of hazardous regions with different heights

Height (m)	1.5	5.0	10	20	30	40
The area of hazardous region (m^2)	4.96	10.95	23.16	76.1	113.61	145.28
Height (m)	50	55	60	65	70	80
The area of hazardous region (m^2)	187.1	200.91	192.53	152.68	108.85	8.69

According to the simulated results, residents who lived in the upper floors of this building group environment should improve their level of emergency response. In addition, evacuation routes and appropriate emergency-management decisions should be provided in advance.

5 Conclusions

In this paper, we validated the CFD methodology which we applied to simulate the wind field and the concentration field based on data from previous field tests and wind tunnel experiments. Then, we created a 3D numerical model to simulate the pressure, wind, and concentration of gas dispersion at the street intersection of a building group. The conclusions are summarized as follows:

(1) We applied the Realizable k-ε model to simulate the turbulent flow surrounding the TTU building. The mean relative error of the mean pressure coefficients was 25.8%

and 28.0%, when comparing the simulated results with field tests and wind tunnel experiments, respectively. The results showed that the mean pressure coefficients were positive on the windward side of the building, whereas they were negative on the top surface and leeward side of the building.

(2) We applied the species transport model to simulate the concentration of gas dispersion in the street canyon. We controlled the boundary parameter variation by user-defined functions during the simulation. The maximum relative error was 21.12%, and the average relative error was less than 12.15%. The results of the concentration field agreed well with the wind tunnel experiments. The numerical approach applicable to simulate gas dispersion was validated.

(3) Influenced by a building group at the street intersection, several different sizes of vortexes, low-wind-speed regions, and negative pressure regions formed under perpendicular wind flow. The wind speed increased when the approach flow passed between buildings on both sides of the road; the case study showed that the wind speed increased in the range from 2.5 m/s to 4 m/s, and even to 4.5 m/s.

(4) In the initial stage, the natural gas dispersion was in front of the downwind direction. As leakage time increased, the gas dispersion was trapped easily in the areas near the leak's origin, vortexes regions, low-wind-speed regions downwind of the leak's origin, and negative pressure regions. Thus, the area and direction of gas dispersion could be anticipated according to the simulated results of the pressure field and the wind field.

(5) The area of hazardous region tended to increase first and then to drop with the dispersion height at the street intersection of a building group. According to the simulated results, the area of hazardous region above 100 m^2 was distributed mainly between the heights of 30 m and 70 m. The maximum area of the hazardous region was 200 m^2 and was located at a height of 55 m, which was in the middle of the computational domain. Therefore, residents who lived in the upper floors should improve the level of their emergency response.

Acknowledgement: This research was supported by the Joint Project of Beijing Municipal Education Commission (No. ZX20140289). Additionally, the authors are grateful to the LetPub and anonymous reviewers for their valuable comments and helpful suggestions to improve the quality of this manuscript.

Funding Statement: The authors received no specific funding for this study.

Conflicts of Interest: The authors declare that they have no conflicts of interest to report regarding the present study.

References

Ahmed, L.; Bengherbia, T.; Zhvansky, R.; Ferrara, G.; Wen, J. X. et al. (2016): Validation of geometry modelling approaches for offshore gas dispersion simulations. *Journal of Loss Prevention in the Process Industries*, vol. 44, pp. 594-600.

Bonnaud, C.; Cluzel, V.; Corcoles, P.; Dubois, J. P.; Louvet, V. et al. (2018):

Experimental study and modelling of the consequences of small leaks on buried transmission gas pipeline. *Journal of Loss Prevention in the Process Industries*, vol. 55, pp. 303-312.

Deng, Y.; Hou, H.; Fang, L.; Yuan, Q.; Yu, B. et al. (2017): Numerical simulation on the dispersion of natural gas release from a buried pipeline. *Heat Transfer Engineering*, vol. 39, no. 7-8, pp. 687-689.

Deng, Y.; Hu, H.; Yu, B.; Sun, D.; Hou, L. et al. (2018): A method for simulating the release of natural gas from the rupture of high-pressure pipelines in any terrain. *Journal of Hazardous Materials*, vol. 342, pp. 418-428.

Ebrahimi-Moghadam, A.; Farzaneh-Gord, M.; Arabkoohsar, A.; Moghadam, A. J. (2018): CFD analysis of natural gas emission from damaged pipelines: correlation development for leakage estimation. *Journal of Cleaner Production*, vol. 199, pp. 257-271.

Ebrahimi-Moghadam, A.; Farzaneh-Gord, M.; Deymi-Dashtebayaz, M. (2016): Correlations for estimating natural gas leakage from above-ground and buried urban distribution pipelines. *Journal of Natural Gas Science and Engineering*, vol. 34, pp. 185-196.

Endo, M.; Bienkiewicz, B.; Ham, H. J. (2006): Wind-tunnel investigation of point pressure on TTU test building. *Journal of Wind Engineering and Industrial Aerodynamics*, vol. 94, no. 7, pp. 553-578.

Foissac, A.; Benoit, L.; Blanchetiere, V.; Geniaut, B.; Zarea, M. et al. (2014): Gas migration in soil from a distribution network leakage: an experimental and numerical study to assess time and spatial scales. *International Gas Union Research Conference*.

Guo, D.; Zhao, P.; Wang, R.; Yao, R.; Hu, J. (2019): Numerical simulation studies of the effect of atmospheric stratification on the dispersion of LNG vapor released from the top of a storage tank. *Journal of Loss Prevention in the Process Industries*, vol. 61, pp. 275-286.

Han, Z. Y.; Weng, W. G. (2011): Comparison study on qualitative and quantitative risk assessment methods for urban natural gas pipeline network. *Journal of Hazardous Materials*, vol. 189, no. 1-2, pp. 509-518.

Houssin-Agbomson, D.; Blanchetière, G.; McCollum, D.; Macary, C. S.; Mendes, R. F. et al. (2018): Consequences of a 12-mm diameter high pressure gas release on a buried pipeline. Experimental setup and results. *Journal of Loss Prevention in the Process Industries*, vol. 54, pp. 183-189.

Kastner-Klein, P.; Plate, E. J. (1999): Wind-tunnel study of concentration fields in street canyons. *Atmospheric Environment*, vol. 33, no. 24-25, pp. 3973-3979.

Lateb, M.; Masson, C.; Stathopoulos, T.; Bédard, C. (2013): Comparison of various types of k-ε models for pollutant emissions around a two-building configuration. *Journal of Wind Engineering and Industrial Aerodynamics*, vol. 115, pp. 9-21.

Levitan, M. L.; Mehta, K. C. (1992): Texas Tech field experiments for wind loads part 1: building and pressure measuring system. *Journal of Wind Engineering and Industrial Aerodynamics*, vol. 43, no. 1-3, pp. 1565-1576.

Li, F.; Wang, W. H.; Dubljevic, S.; Khan, F.; Xu, J. et al. (2019): Analysis on accident-causing factors of urban buried gas pipeline network by combining DEMATEL, ISM and BN methods. *Journal of Loss Prevention in the Process Industries*, vol. 61, pp. 49-57.

Li, Z. G.; Cheng, H.; Gu, T. Y. (2019): Research on dynamic relationship between natural gas consumption and economic growth in China. *Structural Change and Economic Dynamic*, vol. 49, pp. 334-339.

Liu, A.; Huang, J.; Li, Z.; Chen, J.; Huang, X. et al. (2018): Numerical simulation and experiment on the law of urban natural gas leakage and diffusion for different building layouts. *Journal of Natural Gas Science and Engineering*, vol. 54, pp. 1-10.

Liu, B.; Liu, X.; Lu, C.; Godbole, A.; Michal, G. et al. (2016): Computational fluid dynamics simulation of carbon dioxide dispersion in a complex environment. *Journal of Loss Prevention in the Process Industries*, vol. 40, pp. 419-432.

Lu, H. F.; Ma, X.; Azimi, M. (2020): US natural gas consumption prediction using an improved kernel-based nonlinear extension of the Arps decline model. *Energy*, vol. 194, 116905.

Mao, N.; Wang, Z.; Zhou, C.; Tong, X. (2019): Qualitative and quantitative investigation on concentration of indoor dense gas caused by leakage and diffusion. *Environmental Progress & Sustainable Energy*, vol. 38, 12995.

NIGC (2019): Natural gas distribution and consumption. http://www.iraniangas.ir/index.aspx?fkeyid=&siteid=3&pageid=393&newsview=1225.

Okamoto, H.; Gomi, Y. (2011): Empirical research on diffusion behavior of leaked gas in the ground. *Journal of Loss Prevention in the Process Industries*, vol. 24, no. 5, pp. 531-540.

Selvam, R. P. (1997): Computation of pressures on Texas Tech University building using large eddy simulation. *Journal of Wind Engineering and Industrial Aerodynamics*, vol. 67-68, pp. 647-657.

Tauseef, S. M.; Rashtchian, D.; Abbasi, S. A. (2011): CFD-based simulation of dense gas dispersion in presence of obstacles. *Journal of Loss Prevention in the Process Industries*, vol. 24, no. 4, pp. 371-376.

Wang, K.; Shi, T.; He, Y.; Li, M.; Qian, X. (2019): Case analysis and CFD numerical study on gas explosion and damage processing caused by aging urban subsurface pipeline failures. *Engineering Failure Analysis*, vol. 97, pp. 201-219.

Wang, T.; Lin, B. Q. (2017): China's natural gas consumption peak and factors analysis: a regional perspective. *Journal of Cleaner Production*, vol. 142, pp. 548-564.

Zhu, H.; Mao, Z.; Wang, Q.; Sun, J. (2013): The influences of key factors on the consequences following the natural gas leakage from pipeline. *Procedia Engineering*, vol. 62, pp. 592-601.